



Research article

Carrier-microencapsulation of arsenopyrite using Al-catecholate complex: nature of oxidation products, effects on anodic and cathodic reactions, and coating stability under simulated weathering conditions

Ilhwan Park^{a,*}, Carlito Baltazar Tabelin^b, Kensuke Seno^c, Sanghee Jeon^a, Hiroyuki Inano^d, Mayumi Ito^a, Naoki Hiroyoshi^a^a Division of Sustainable Resources Engineering, Faculty of Engineering, Hokkaido University, Sapporo, 060-8628, Japan^b School of Minerals and Energy Resources Engineering, The University of New South Wales, Sydney, NSW, 2052, Australia^c Division of Sustainable Resources Engineering, Graduate School of Engineering, Hokkaido University, Sapporo, 060-8628, Japan^d Hokkaido Research Organization Industrial Research Institute, Sapporo, 060-0819, Japan

ARTICLE INFO

Keywords:

Chemical engineering
Environmental science
Acid mine drainage
Arsenopyrite
Electrochemical studies
Microencapsulation
Stability tests

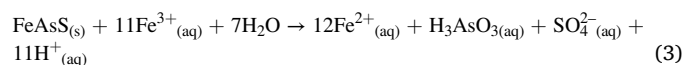
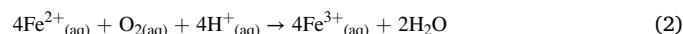
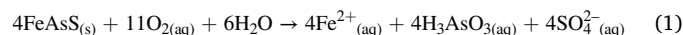
ABSTRACT

Mining activities often generate large amounts of sulfide-rich wastes containing arsenopyrite (FeAsS), which when dissolved releases toxic arsenic (As) and generates acid mine drainage (AMD) that are both disastrous to the environment. To suppress arsenopyrite dissolution, a technique that selectively coats sulfide minerals with a protective layer of Al-oxyhydroxide called Al-based carrier-microencapsulation (CME) was developed. Although a previous study of the authors showed that Al-based CME could significantly limit arsenopyrite dissolution, nature of the coating formed on arsenopyrite, including its electrochemical properties, is still not well understood. Moreover, stability of the coating once exposed to weathering conditions remains unclear. Better understanding of these important issues would greatly improve Al-based CME especially in its application to real mine wastes. In this study, nature of the coating formed by Al-based CME was investigated using SEM-EDX, DRIFTS and XPS while the electrochemical properties of the coating were evaluated by cyclic voltammetry and chronoamperometry. Meanwhile, stability of the coating was elucidated using consecutive batch leaching experiments and weathering cell tests.

SEM-EDX, DRIFTS and XPS results indicate that the protective coating formed on arsenopyrite by Al-based CME was mainly composed of bayerite (α -Al(OH)₃), gibbsite (γ -Al(OH)₃), and boehmite (γ -AlO(OH)). These Al-based coatings, which have insulating properties, made arsenopyrite less electrochemically active. The coatings also limited the extent of both the anodic and cathodic half-cell reactions of arsenopyrite oxidation that suppressed As release and acid generation. Weathering cell tests indicated that the oxidation of CME-treated arsenopyrite was effectively limited until about 15 days but after this, it started to gradually progress with time due to the increasing acidity of the system where Al-based coatings became unstable. Nonetheless, CME-treated arsenopyrite was less oxidized based on the released amounts of Fe, As and S suppressed by 80, 60 and 70%, respectively, compared with the one treated with control.

1. Introduction

Arsenopyrite (FeAsS), the most common arsenic (As)-bearing sulfide mineral in nature, releases toxic As into the surrounding environment when exposed to atmospheric conditions according to the following reactions (Corkhill and Vaughan, 2009; Dos Santos et al., 2016; Murciago et al., 2011):



The predominant As species found in contaminated waters and acid mine drainage (AMD) are arsenite (As³⁺) and arsenate (As⁵⁺), both of which are highly soluble and mobile over a wide range of pH and Eh

* Corresponding author.

E-mail address: i-park@eng.hokudai.ac.jp (I. Park).

conditions (Park et al., 2018a, 2019a; Tabein et al., 2010, 2012a, b, 2014a, 2017a, b). Arsenic is a toxic metalloid known to cause numerous diseases like hyperpigmentation, keratosis, anemia, and neuropathy as well as the increased risk of developing several types of cancers even at minute amounts (i.e., $\mu\text{g/L}$ levels) when ingested continuously for prolonged periods of time (i.e., chronic poisoning) (Duker et al., 2005; Mohan and Pittman, 2007; Park et al., 2019b; Seno et al., 2019; Tabein et al., 2018). Like pyrite (FeS_2), the oxidation of arsenopyrite also generates AMD. In fact, arsenopyrite has a stronger acidification potential than pyrite; that is, when both minerals are exposed to the environment, acidity production from arsenopyrite is almost three times higher than that of pyrite (Abbassi et al., 2009; Chopard et al., 2017). Highly contaminated leachates, including AMD, acid rock drainage (ARD) and neutral mine drainage (NMD), are notorious environmental problems encountered not only by the mining and mineral processing industries but also in underground construction projects for roads, railways, hydroelectric powerplants and shopping malls (Igarashi et al., 2008; Herrera et al., 2007; Li et al., 2016; Tabein et al., 2013, 2014b; Tamoto et al., 2015; Tatsuhara et al., 2012). This is primarily because AMD/ARD is very acidic (typically with pH less than 3) and contains high amounts of hazardous heavy metals (e.g., copper (Cu), iron (Fe), manganese (Mn), lead (Pb), and zinc (Zn)) (Johnson and Hallberg, 2005; Park et al., 2018b, 2019a) and toxic metalloids (e.g., As and selenium (Se)) (Tabelin and Igarashi, 2009; Tabein et al., 2012c, d).

The most common technique used to mitigate the negative environmental impacts of AMD is through neutralization, an approach whereby alkaline materials like limestone (CaCO_3), quicklime (CaO), or slaked lime (Ca(OH)_2) are added to raise the pH of AMD, thereby precipitating most of the dissolved metals as hydroxides and carbonates (Johnson and Hallberg, 2005). This technique could remediate AMD effectively, but it has two critical limitations: (1) high operating costs due to the continuous input of chemicals and energy until AMD formation stops (Gazee et al., 1996), and (2) disposal of huge amounts of bulky and hazardous sludge produced by the treatment (Kefeni et al., 2015). Because of these limitations of neutralization, alternative strategies that directly passivate sulfide minerals by coating them with surface-protective layers have been proposed in recent years. Collectively referred to as encapsulation techniques, some examples include ferric-phosphate (Huang and Evangelou, 1992; Evangelou, 1995), ferric hydroxide-silica (Evangelou, 1996; Zhang and Evangelou, 1998), silane-based (Khummalai and Boonnamnuayvitaya, 2005; Liu et al., 2017; Ouyang et al., 2015), and organic-based (Acai et al., 2009; Cai et al., 2005; Elsetinow et al., 2003). However, these techniques have some serious drawbacks. The methods forming ferric-phosphate and ferric hydroxide-silica coatings (Huang and Evangelou, 1992; Evangelou, 1995, 1996; Zhang and Evangelou, 1998), for example, require hydrogen peroxide (H_2O_2) as an oxidant, which is not only expensive but also difficult to store and handle for large-scale applications. Similarly, organic-based coatings are only stable for a relatively short period of time because they are degraded by microorganisms, and once the coatings disappear, AMD formation would simply restart. More importantly, all these encapsulation techniques are non-selective, which means that they cannot target sulfide minerals like pyrite and arsenopyrite in complex wastes containing quartz and alumino-silicate minerals. In other words, current encapsulation techniques are impractical for large-scale applications because they require unnecessarily high amounts of expensive chemicals to work. To overcome these limitations, the authors developed a new passivation technique called carrier-microencapsulation (CME) (Jha et al., 2008; Li et al., 2019; Park et al., 2018c, d; Satur et al., 2007). In CME, redox-sensitive metal(loid)-organic complexes are mixed with AMD-forming minerals like pyrite and arsenopyrite to oxidatively decompose these complexes and release their metal(loid) ion loads, which are then precipitated on sulfide minerals to form the coating. Because the dissolutions of pyrite and arsenopyrite are electrochemical in nature (Crundwell, 1988; Rimstidt and Vaughan, 2003; Tabein et al., 2017c, d), decomposition of the metal(loid) complexes occurs preferentially on surfaces of these minerals

and not on the silicate-bearing mineral matrix, so CME can specifically target AMD-generating minerals even in complex systems like mine tailings and waste rocks.

Among the complexes evaluated for CME, Al(III) mono-catecholate complex (i.e., $[\text{Al}(\text{cat})]^+$) was the most practical because of the following reasons: (1) $[\text{Al}(\text{cat})]^+$ decomposition is faster (<3 days) than Ti-catecholate complex (>14 days) (Park et al., 2018c), (2) Si-catecholate complex can be synthesized only at high concentration of catechol (i.e., $\text{H}_2\text{cat}/\text{Si}^{4+} > 9$) (Park et al., 2018d), and (3) the suppressive effects of $[\text{Al}(\text{cat})]^+$ were better than Fe(III)-catecholate complexes ($[\text{Fe}(\text{cat})_n]^{3-2n}$, where n is 1–3) (Li et al., 2019). Although CME using Al-catecholate complex (i.e., Al-based CME) effectively suppressed arsenopyrite oxidation, nature of the coating formed on the mineral surface, its redox properties, and stability during prolonged exposure to the environment are still not well understood. In addition, the mechanisms of how the coating suppressed arsenopyrite oxidation in Al-based CME remain unclear. Hence, this study aims to: (1) characterize the coating formed on arsenopyrite in Al-based CME by scanning electron microscopy with energy dispersive X-ray spectroscopy (SEM-EDX), diffuse reflectance infrared Fourier transform spectroscopy (DRIFTS), and X-ray photoelectron spectroscopy (XPS), (2) investigate changes in electrochemical properties of Al-based CME-treated arsenopyrite using cyclic voltammetry (CV) and chronoamperometry, and (3) evaluate the stability of CME-treated arsenopyrite under simulated weathering conditions by consecutive batch leaching experiments and weathering cell tests.

2. Materials and methods

2.1. Sample characterization

The arsenopyrite sample used in this study was obtained from Toroku mine, Miyazaki, Japan. It was crushed with a jaw crusher (BB 51, Retsch Inc., Germany), ground in a vibratory disc mill (RS 100, Retsch Inc., Germany), and then screened to obtain a size fraction of 100–150 μm . X-ray powder diffraction (XRD, MultiFlex, Rigaku Corporation, Japan) confirmed that the sample is mainly composed of arsenopyrite with pyrite and quartz as minor mineral impurities (Park et al., 2018c). Moreover, the sample is composed of 32.6% Fe, 30.9% As and 20.1% S, which are roughly equivalent to 67% arsenopyrite, 13% pyrite and 15% quartz (Park et al., 2018c).

2.2. Al-based CME treatment of arsenopyrite

Arsenopyrite samples were treated by Al-based CME using a solution containing 15 mM of $\text{AlCl}_3 \cdot 6\text{H}_2\text{O}$ and 15 mM of catechol (1,2-dihydroxybenzene, $\text{C}_6\text{H}_4(\text{OH})_2$) and for reference, control experiments were done using deionized (DI) water with 45 mM NaCl. Both solutions were adjusted to pH 5 using dilute NaOH solution. In the control, NaCl was added to normalize the effects of Cl^- on arsenopyrite oxidation because the source of Al^{3+} for the CME solution was AlCl_3 . All chemicals used in this study were of reagent grade (Wako Pure Chemical Industries, Ltd., Japan). For these experiments, 1 g of arsenopyrite (100–150 μm) and 10 mL of prepared solution were put into a 50-mL Erlenmeyer flask and then mixed at 120 min^{-1} in a constant temperature water bath shaker (25°C) for 3 days. After this, the CME-treated arsenopyrite and control were collected by vacuum filtration (0.2 μm membrane filter), rinsed with DI water six times, dried in a vacuum drying oven at 40°C for 1 day, and analyzed by SEM-EDX (JSM-IT200, JEOL Ltd., Japan), DRIFTS (FT/IR-6200HFV with DR PR0410-M attachment, Jasco Analytical Instruments, Japan), and XPS (Axis-His, Shimadzu/Kratos Corporation, Japan). The XPS analysis was conducted under ultrahigh vacuum conditions (approximately 8×10^{-8} torr) using a monochromatized Al $K\alpha$ X-ray source (1486.7 eV) operated at 140 W (Voltage, 14 kV; Current, 10 mA). Narrow scan spectra of Fe 2p_{3/2}, As 3d_{5/2}, S 2p_{3/2}, Al 2p_{3/2}, and O 1s were obtained and calibrated using the binding energy of adventitious carbon (C 1s) (285.0 eV) for charge correction. All XPS data were analyzed by XPSPEAK version 4.1 and deconvolutions of the spectra were

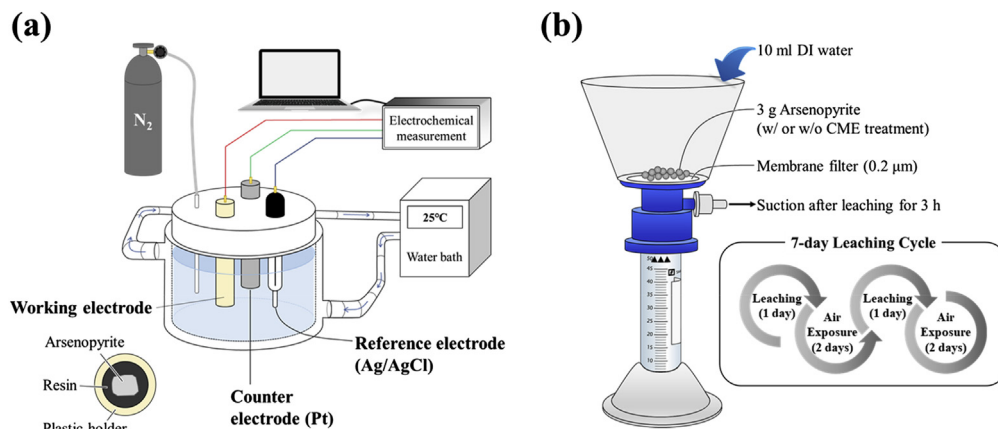


Figure 1. The schematic diagrams of experimental setup for (a) electrochemical studies and (b) weathering cell tests.

done using a 80% Gaussian–20% Lorentzian peak model and a true Shirley background (Nesbitt and Muir, 1994; Shirley, 1972).

2.3. Electrochemical studies

A large, single crystal arsenopyrite sample obtained from Yaogangxian mine, Hunan, China was used to prepare the working electrode. A cuboid was cut from the mineral sample using a diamond cutter, connected to copper wires using silver conducting paste (DOTITE, Fujikura Kasei Co., Ltd., Japan), and fixed inside a plastic holder using Technovit® non-conductive resin (Heraeus Kulzer GmbH, Germany). To expose the surface of arsenopyrite, the electrode was polished with silicon carbide papers (#200→#600→#1200→#1500) and alumina (Al_2O_3) pastes (5 and 1 μm). After this, the polished electrode was cleaned using an ultrasonicator (W-113, Honda Electronics Co., Ltd., Japan) for 5 min to remove residual Al_2O_3 particles and then washed thoroughly with DI water.

The polished arsenopyrite electrode was treated in a magnetically stirred (200 rpm) solution of either 45 mM NaCl (control) or 15 mM $[\text{Al}(\text{cat})]^+$ solution (Al-based CME) at room temperature for 3 days. After this, the pretreated electrode was thoroughly washed with DI water, dried under ambient conditions for 1 h and then used in the electrochemical measurements.

Cyclic voltammetry (CV) was carried out using an SI 1280B electrochemical measurement unit (Solartron Instruments, UK) with a standard three-electrode cell setup (Figure 1a). Arsenopyrite electrode, platinum (Pt) electrode and Ag/AgCl electrode filled with saturated KCl were used as working, counter and reference electrodes, respectively. For the electrochemical measurements, an electrolyte solution containing 0.1 M Na_2SO_4 was prepared, equilibrated at 25 °C, and deoxygenated by N_2 purging for 30 min. After insertion of the working electrode into the cell, the system was equilibrated at the open circuit potential (OCP) and then CV measurements were done between -0.6 and 1.0 V vs. SHE at a scan rate of 30 mV/s.

Chronoamperometry was conducted to identify the effects of coatings formed by Al-based CME on the anodic and cathodic half-cell reactions of arsenopyrite oxidation. A setup similar to the CV measurements was used but with stirring at 250 rpm. After equilibration at the OCP, the working electrode was polarized at 0.0 V for the cathodic polarization measurements (without N_2 purging) and at +0.8 V for the anodic polarization measurements (with N_2 purging). These polarization potentials were selected because according to Almeida and Giannetti (2003) and Urbano et al. (2008), arsenopyrite was anodically and irreversibly oxidized at +0.8 V while at 0.0 V, the cathodic reaction occurred without interference from the reductive dissociation of the mineral.

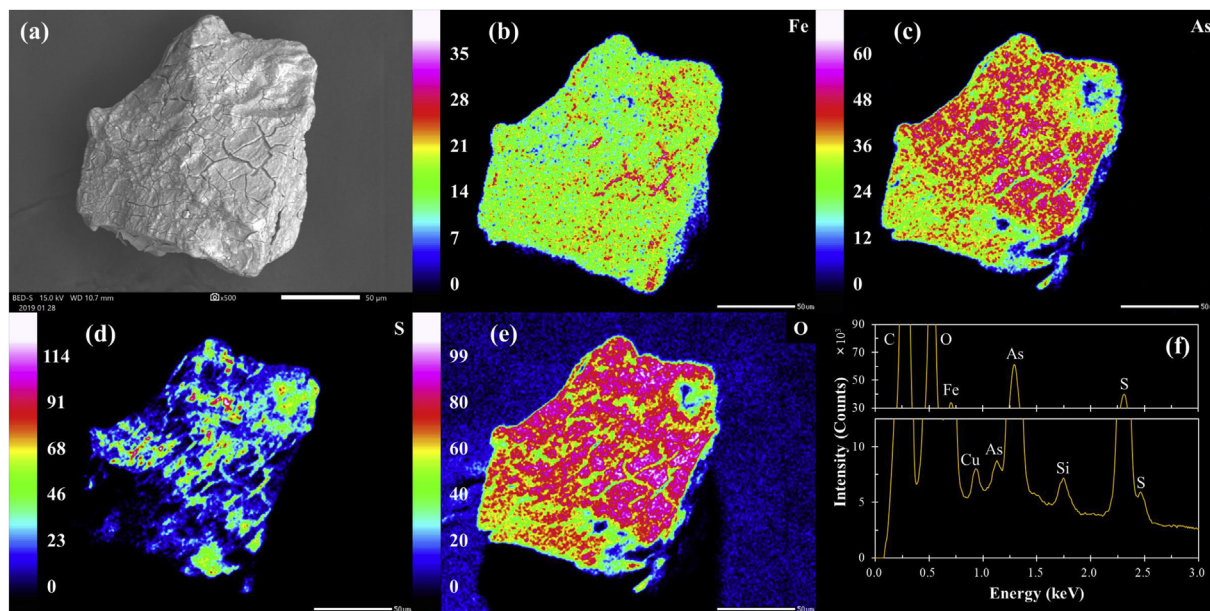


Figure 2. SEM-EDX analysis of arsenopyrite in the control experiments: (a) SEM photomicrograph, elemental maps of (b) Fe, (c) As, (d) S and (e) O, and (f) energy dispersive X-ray spectrum of the scanned area.

Table 1. XPS peak parameters for Fe 2p, As 3d, S 2p, O 1s, and Al 2p spectra.

Spectral peak	Binding energy (eV)	FWHM	Chemical states
Fe 2p _{3/2} ^a	707.1 ± 0.1	1.00	Fe(II)-AsS
Fe 2p _{3/2} ^b	709.7 ± 0.1	1.30	Fe(III)-AsS
Fe 2p _{3/2} ^b	711.2 ± 0.1	1.50	Fe(III)-O
As 3d _{5/2} ^c	40.9 ± 0.1	1.00	As(-I)-S
As 3d _{5/2c}	41.5 ± 0.1	1.00	As(0)
As 3d _{5/2} ^c	43.6 ± 0.1	0.95	As(I)-O
As 3d _{5/2} ^c	44.4 ± 0.2	0.95	As(III)-O
As 3d _{5/2} ^c	45.4 ± 0.3	0.95	As(V)-O
S 2p _{3/2} ^d	161.4 ± 0.3	1.2	Monosulfide (S ²⁻)
S 2p _{3/2} ^d	162.0 ± 0.1	1.0	Disulfide (S ₂ ²⁻)
S 2p _{3/2} ^d	163.0 ± 0.2	1.6	Polysulfide (S _n ²⁻)
S 2p _{3/2} ^d	166.3 ± 0.1	1.2	Thiosulfate (SO ₃ ²⁻)
S 2p _{3/2} ^d	167.2 ± 0.2	1.2	Sulfate (SO ₄ ²⁻)
O 1s	531.0 ± 0.2	1.6	Lattice oxygen (O ²⁻)
O 1s	532.0 ± 0.3	1.6	Hydroxyl oxygen (OH ⁻)
O 1s	533.2 ± 0.5	1.6	Attached water (H ₂ O)
Al 2p _{3/2}	73.9 ± 0.1	1.0	Al-O in boehmite
Al 2p _{3/2}	74.3 ± 0.1	1.0	Al-OH in bayerite & gibbsite
Al 2p _{3/2}	74.8 ± 0.1	1.0	Al-OH in bayerite

^a This peak has two multiplets located at lower and higher binding energies with 0.95 eV peak separation.

^b This peak has three multiplets located at higher binding energies with 0.95 eV peak separation.

^c This peak has a doublet located at a higher binding energy with 0.7 eV peak separation. The intensity ratio was constrained to two thirds with the same FWHM.

^d This peak has a doublet located at a higher binding energy with 1.18 eV peak separation. The intensity ratio was constrained to one half with the same FWHM.

2.4. Consecutive batch leaching experiments

Consecutive batch leaching experiments were designed for the prolonged leaching of environmentally regulated elements in contaminated soils, sediments, rocks and wastes that roughly approximates the behavior of contaminants in column experiments (Tabelin et al., 2014c).

Because of this, the method is also appropriate for the evaluation of coating stability after CME treatment of arsenopyrite samples. In these experiments, 1 g of treated sample and 10 mL of DI water were put in a 50-mL conical centrifuge tube and then shaken in a constant temperature water bath shaker (25 °C) at 120 min⁻¹ for 24 h. The suspension was then centrifuged at 3500 rpm for 20 min to separate the supernatant and solid residue. The supernatant was collected by decantation, filtered through 0.2 μm syringe-driven membrane filter (LMS Co. Ltd., Japan), and analyzed by an inductively coupled plasma atomic emission spectrometer (ICPE-9820, Shimadzu Corporation, Japan) (margin of error ± 2%) while the solid residue was leached again with 10 mL of DI water. These series of leaching-centrifugation-filtration steps were repeated five times.

2.5. Weathering cell tests

The long-term stability of CME-treated arsenopyrite was evaluated using weathering cell tests based on the procedure of Bouzahzah et al. (2014). For these tests, control and CME-treated samples were placed on 50-mm diameter Büchner funnels with 0.2 μm membrane filters connected to centrifuge tubes (Figure 1b). A 7-day leaching cycle was adopted in this study as follows: leaching with DI water on day 1 → exposure to ambient conditions on days 2 and 3 → leaching with DI water on day 4 → exposure to ambient conditions on days 5–7. The amount of sample placed in the weathering cells and the volume of DI water poured were 3 g and 10 mL, respectively. During days 1 and 4 (leaching day), 10 mL of DI water was poured in the weathering cell that submerged the sample for 3 h. After this, the weathering cell was connected to a vacuum pump to collect the leachate, which was then filtered through 0.2 μm syringe-driven membrane filter and immediately analyzed by ICP-AES. At the end of the weathering cell tests, the residues were rinsed with DI water six times, dried in a vacuum drying oven at 40 °C for 1 day and then analyzed by DRIFTS.

3. Results and discussion

3.1. Surface characterizations of treated arsenopyrite

Figure 2 shows the SEM-EDX results of arsenopyrite treated in NaCl solution for 3 days (i.e., control). The SEM photomicrograph of arsenopyrite in the control experiment had a “cracky” surface morphology,

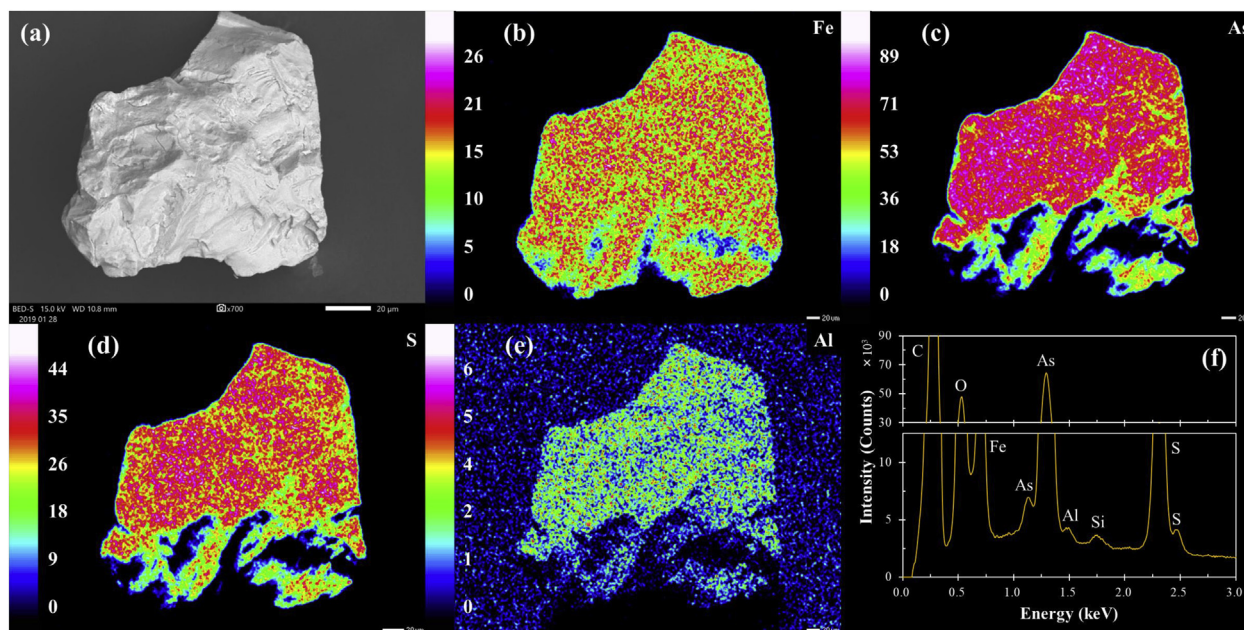


Figure 3. SEM-EDX analysis of Al-based CME-treated arsenopyrite: (a) SEM photomicrograph, elemental maps of (b) Fe, (c) As, (d) S and (e) Al, and (f) energy dispersive X-ray spectrum of the scanned area.

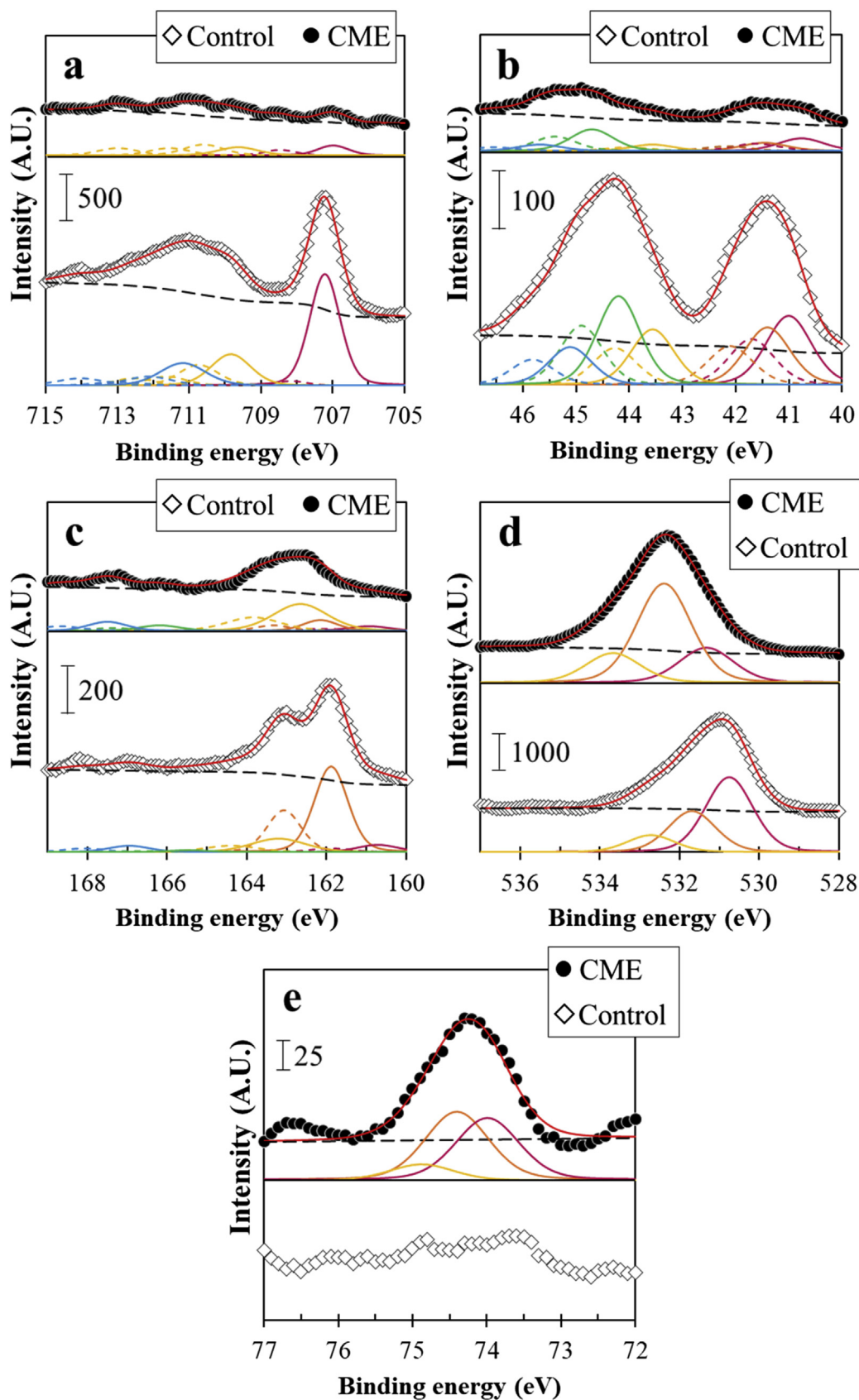


Figure 4. XPS spectra of arsenopyrite treated in the control and by Al-based CME: (a) Fe 2p_{3/2}, (b) As 3d_{5/2}, (c) S 2p_{3/2}, (d) O 1s, and (e) Al 2p_{3/2}.

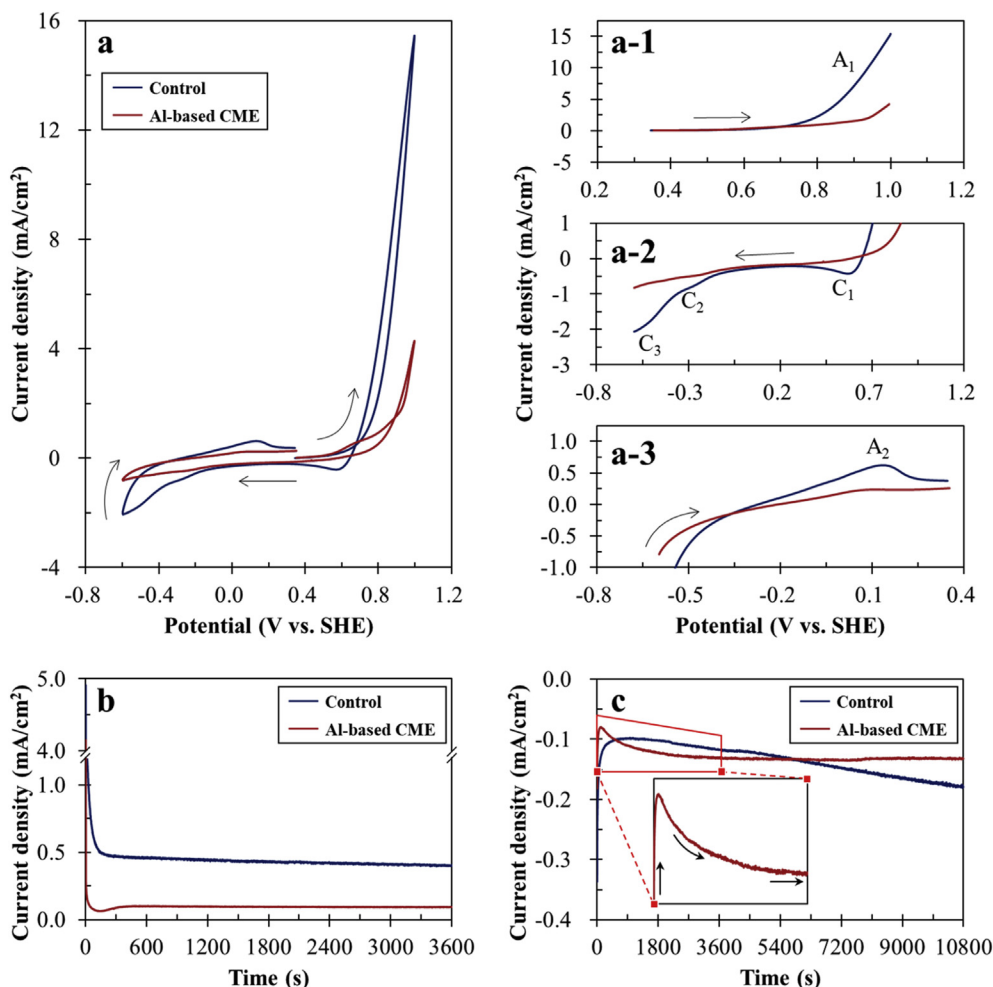


Figure 5. (a) Cyclic voltammograms of arsenopyrite treated in the control and by Al-based CME: (a-1) anodic sweep from OCP to +1.0 V, (a-2) cathodic sweep from +1.0 to -0.6 V, and (a-3) anodic sweep from -0.6 V to OCP. The chronoamperometric response of arsenopyrite treated in the control and by Al-based CME: (b) anodic polarization at an applied potential of +0.8 V, and (c) cathodic polarization at an applied potential of 0.0 V. Note that arrows in Figure 4a denote the sweep direction.

which was mainly composed of Fe, As, S, and O based on the EDX maps and spectrum (Figure 2). To identify the nature of this “cracky” layer in more detail, arsenopyrite in the control experiment was examined by XPS. The XPS spectra of Fe 2p_{3/2}, As 3d_{5/2}, S 2p_{3/2}, O 1s, and Al 2p_{3/2} are shown in Figure 4 and the corresponding curve fitting parameters are summarized in Table 1. The Fe 2p_{3/2} spectrum (Figure 4a) shows one strong peak at 707.3 eV, which could be attributed to Fe(II)–AsS in mineral lattices (Corkhill and Vaughan, 2009; Lara et al., 2016; Nesbitt et al., 1995; Zhu et al., 2014). There is another broad peak centered at around 711 eV, which when deconvoluted revealed multiple peaks of Fe(III) species like Fe(III)–AsS and Fe(III)–O. Likewise, the XPS spectra of As 3d_{5/2} and S 2p_{3/2} also show several peaks of oxidized species of As (e.g., As(0), As(I)–O, As(III)–O, and As(V)–O) and S (e.g., S_n²⁻, SO₃²⁻, and SO₄²⁻) (Figures 4b and c). Fe, As and S in unoxidized arsenopyrite occur in the (+2), (-1) and (-1) oxidation states, respectively, so the extent of their oxidations in the control experiment could be calculated by integrating each oxidized species based on the XPS fitting data as explained by the following equations (Zhu et al., 2014):

$$\text{Fe}_{\text{tot-ox}} = \text{Fe(III)-AsS} + \text{Fe(III)-O} \quad (4)$$

$$\text{As}_{\text{tot-ox}} = \text{As(0)} + \text{As(I)-O} + \text{As(III)-O} + \text{As(V)-O} \quad (5)$$

$$\text{S}_{\text{tot-ox}} = \text{S}_n^{2-} + \text{SO}_3^{2-} + \text{SO}_4^{2-} \quad (6)$$

where “tot-ox” denotes the total amount of oxidized species in the outermost surface of the oxidation layer. The calculation revealed that

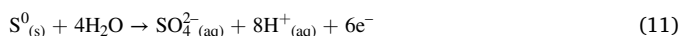
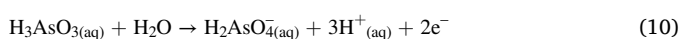
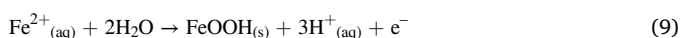
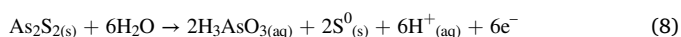
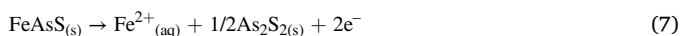
the total percentage of oxidized Fe, As and S were around 57, 77 and 27 at.%, respectively. This means that for arsenopyrite, the oxidation preference of its constituent elements follows this order: As > Fe > S and is consistent with the observations of Buckley and Walker (1988). The XPS spectrum of O 1s (Figure 4d) also implies that arsenopyrite oxidation was quite extensive because of the peaks assigned to lattice oxygen (O²⁻), hydroxyl oxygen (OH⁻), and attached water (H₂O). The presence of Fe 2p_{3/2} peak at 711.2 eV with its multiplets, attributed to Fe(III)–O binding energies, and the O 1s peak at 531.0 eV (O²⁻) implies that the oxidation products formed on the surface of arsenopyrite in the control experiment were mainly composed of iron(III)-oxyhydroxides (goethite, α-FeO(OH)) (Abdel-Samad and Watson, 1997; Ding et al., 2000; Frau et al., 2005; Huo et al., 2017). Moreover, the O 1s spectrum peak at 532.0 eV could be assigned to OH⁻ that is coordinated with adsorbed As^{III/V} on iron(III)-oxyhydroxide (Ding et al., 2000; Nesbitt et al., 1995).

In comparison, the SEM photomicrograph of Al-based CME-treated arsenopyrite shows the absence of a “cracky” surface morphology and surface composition of the CME-treated arsenopyrite is comprised of not only Fe, As, S, and O but also Al (Figure 3). The XPS spectra of Fe 2p_{3/2}, As 3d_{5/2}, and S 2p_{3/2} indicate that oxidation products were still present on arsenopyrite, but their relative abundances were much lower than in the control as implied by their weaker intensities (Figure 4a–c). One possible explanation for these differences is the formation of another kind of layer on the surface of arsenopyrite. As shown in the XPS spectrum of Al 2p_{3/2}, CME-treated arsenopyrite has

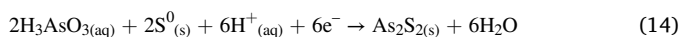
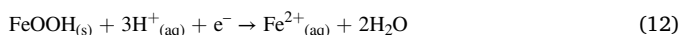
three distinct peaks at 73.9, 74.3, and 74.8 eV, while those were absent in the spectrum of arsenopyrite in the control experiment (Figure 4e). According to Klopogge and Wood (2016) and Klopogge et al. (2006) who analyzed a variety of Al-bearing minerals by XPS, the Al 2p_{3/2} spectrum peaks observed in CME-treated arsenopyrite imply that the coatings on arsenopyrite are most likely composed of bayerite (α-Al(OH)₃), gibbsite (γ-Al(OH)₃) and boehmite (γ-AlO(OH)). The peak observed at 73.9 eV is attributed to the binding energy of boehmite, while both bayerite and gibbsite show the XPS peak at 74.3 eV due to their similarity; however, bayerite has a tailed-peak at 74.8 eV (Klopogge et al., 2006). Bayerite is a metastable monoclinic mineral and is an intermediate product between amorphous Al(OH)₃·nH₂O and gibbsite (Ruan et al., 2001). Thus, the possible mechanism of the formation of Al-based coatings is most likely as follows: (1) [Al(cat)]⁺ decomposition that releases Al³⁺, (2) formation of amorphous Al(OH)₃, and (3) transformation of amorphous Al(OH)₃ to bayerite → gibbsite → boehmite (Elderfield and Hem, 1973; Hsu, 1966; Lee et al., 1999; Violante and Huang, 1993).

3.2. Electrochemical properties of arsenopyrite after treatment

Arsenopyrite dissolution occurs via an electrochemical mechanism wherein distinct anodic and cathodic half-cell reactions occur through the movement of electrons in the mineral's crystal lattice (Walker et al., 2006). Understanding how the electrochemical properties of arsenopyrite changed due to the oxidation products in the control experiments or the bayerite-gibbsite-boehmite coating could provide insights into the various suppression mechanisms of Al-based CME. Figure 5a shows the current density profiles measured by CV using arsenopyrite electrode treated in the control and by Al-based CME. In the first anodic sweep of the control, the current density increased drastically above 0.7 V (Figure 5a-1). This increase in current density, denoted as A₁, is most likely the result of several interrelated anodic reactions of arsenopyrite and its oxidation products as illustrated in the following reactions (Almeida and Giannetti, 2003; Urbano et al., 2008):



At the onset of arsenopyrite oxidation, Fe²⁺ is released into solution and a realgar-like (As₂S₂) phase is formed on the surface of arsenopyrite (reaction 7). With increasing applied potential, this realgar-like phase is further oxidized to As(III) species (H₃AsO₃) and elemental sulfur (S⁰) (reaction 8). Finally, the partly oxidized Fe, As and S species are further oxidized to FeOOH, H₂AsO₄⁻, and SO₄²⁻ as the applied potential becomes more positive (reactions 9–11). When the scanning direction was reversed (i.e., cathodic sweep, Figure 5a-2), three distinct peaks (C₁, C₂ and C₃) were observed, which are most likely attributed to the reduction of the products (e.g., Fe(III) and As(V)) formed during the previous anodic scan (reactions 12–14). Moreover, another anodic peak (A₂) appeared at around 0.1 V when the sweep direction was reversed as shown in Figure 5a-3, which could be attributed to the oxidation of realgar-like phase (reaction 8) formed by reaction 14.



Meanwhile, the cyclic voltammogram of CME-treated arsenopyrite shows that Al-based CME significantly changed the electrochemical

properties of arsenopyrite (Figure 5a). Compared with the control, both anodic and cathodic current densities of CME-treated arsenopyrite substantially decreased as illustrated in Figure 5a-1–a-3, indicating that Al-based CME treatment made arsenopyrite less electrochemically active. This could be explained by the difference in the mineral surfaces formed after the treatments. As shown in Figure 2, the oxidation products in the control were cracked and flaky while those after CME treatment were more uniform and smoother with very little cracks (Figure 3). Moreover, Al-oxyhydroxides are known as insulators with low electrical conductivity, so the formation of crack-free bayerite-gibbsite-boehmite coatings on arsenopyrite made it electrochemically inert by increasing the quantum tunneling energy barrier and limiting interconnected charge transport (Heo et al., 2012).

Although CV could provide insights into the redox reactions occurring at the mineral-electrolyte interface, this technique measures electrons generated/removed by surface reactions only for a very short time (i.e., several seconds) (Tabelin et al., 2017d). This means that the half-cell reactions of arsenopyrite oxidation for longer periods of time remain unclear. To better understand the effects of the oxidation layers and bayerite-gibbsite-boehmite coating on the electrochemical dissolution of arsenopyrite, chronoamperometry was used. In this electrochemical technique, a fixed potential is applied to the working electrode and electron transfer between the working and counter electrodes is measured. One advantage of this technique is its ability to decouple anodic and cathodic half-cell reactions and investigate them separately. Figure 5b shows the anodic polarization curves of arsenopyrite electrode treated in control and by Al-based CME. The anodic current density profile of CME-treated arsenopyrite measured was substantially lower than that of the control, which means that the bayerite-gibbsite-boehmite coating suppressed the anodic half-cell reaction of arsenopyrite oxidation (reaction 15). This suppressive effect could be explained by two possible mechanisms: (1) the coating formed by CME treatment limited the contact of arsenopyrite and water, and (2) the CME generated coating inhibited diffusion of reaction products of arsenopyrite oxidation into solution.

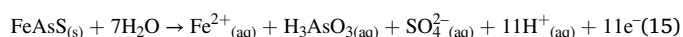


Figure 5c shows the cathodic polarization curves of arsenopyrite electrode treated in control and by Al-based CME. In the control, the cathodic current density profile gradually increased after it decreased rapidly for a short time (ca. 15 min). This trend could be explained by the effects of oxidation products formed on the arsenopyrite electrode. As explained by Figures 2 and 4, the oxidation product formed on arsenopyrite in the control experiment was mainly composed of goethite. Iron(III)-oxyhydroxides like goethite and lepidocrocite (γ-FeOOH) are known to have high electrical resistivities at around 1 × 10⁹ Ω cm (Habib, 2016), so the cathodic reaction of arsenopyrite oxidation (i.e., oxygen reduction expressed by reaction 16) was limited that caused the initial decrease in current density.



At an applied potential of 0.0 V, however, iron(III)-oxyhydroxide could be reductively dissolved (as confirmed by the CV results illustrated in Figure 5a-2) exposing reactive surfaces for oxygen reduction (reaction 16). Because of the combined reduction reactions of goethite (reaction 12) and dissolved oxygen (reaction 16), the cathodic current density profile of arsenopyrite electrode treated in the control increased gradually but continuously. In contrast, the cathodic polarization curve of CME-treated arsenopyrite electrode showed that its current density decreased rapidly and then increased again before it stabilized (Figure 5c). Yuniati et al. (2015) reported that quinone (1,2-benzoquinone, C₆H₄O₂), by-product formed during metal(loid)-catecholate complex decomposition, is adsorbed onto the mineral surface after CME treatment. Adsorbed quinone could be reduced back to catechol at 0.0 V as highlighted by other authors (Li et al., 2019; Park et al., 2018c, d), so

Table 2. Electric charges generated/transferred during the anodic and cathodic polarization measurements of arsenopyrite pretreated in the control and by Al-based CME.

Pretreatment	Electric charge, Q (C/cm ²)	
	Anodic	Cathodic
Control	19.3	9.68
Al-based CME	7.28	7.14

the increase in cathodic current density could be attributed to quinone reduction back to catechol.

The amounts of electric charge generated/transferred during polarization, which were measured by calculating the areas below the current density curves ($Q [C] = I [A] \times t [s]$), are listed in Table 2. Al-based CME treatment suppressed the total amounts of electric charge generated and/or transferred during the anodic and cathodic polarizations by around 62

and 26%, respectively. According to Walker et al. (2006), the rate-determining step of arsenopyrite dissolution was the anodic half-cell reaction, which involves the multi-step oxidation of arsenic and sulfur species. Based on these calculations, the bayerite-gibbsite-boehmite coating formed by Al-based CME could limit arsenopyrite dissolution by at least 60%.

3.3. Stability of Al-based CME-treated arsenopyrite under simulated weathering conditions

Consecutive batch leaching experiments of arsenopyrite treated in the control and by Al-based CME were conducted to evaluate the suppressive effects and stability of coated arsenopyrite. The leachabilities of Fe, As and S in both cases showed linear trends, indicating that arsenopyrite oxidation occurred continuously even after the mineral was coated with a bayerite-gibbsite-boehmite layer by Al-based CME (Figure 6a–c).

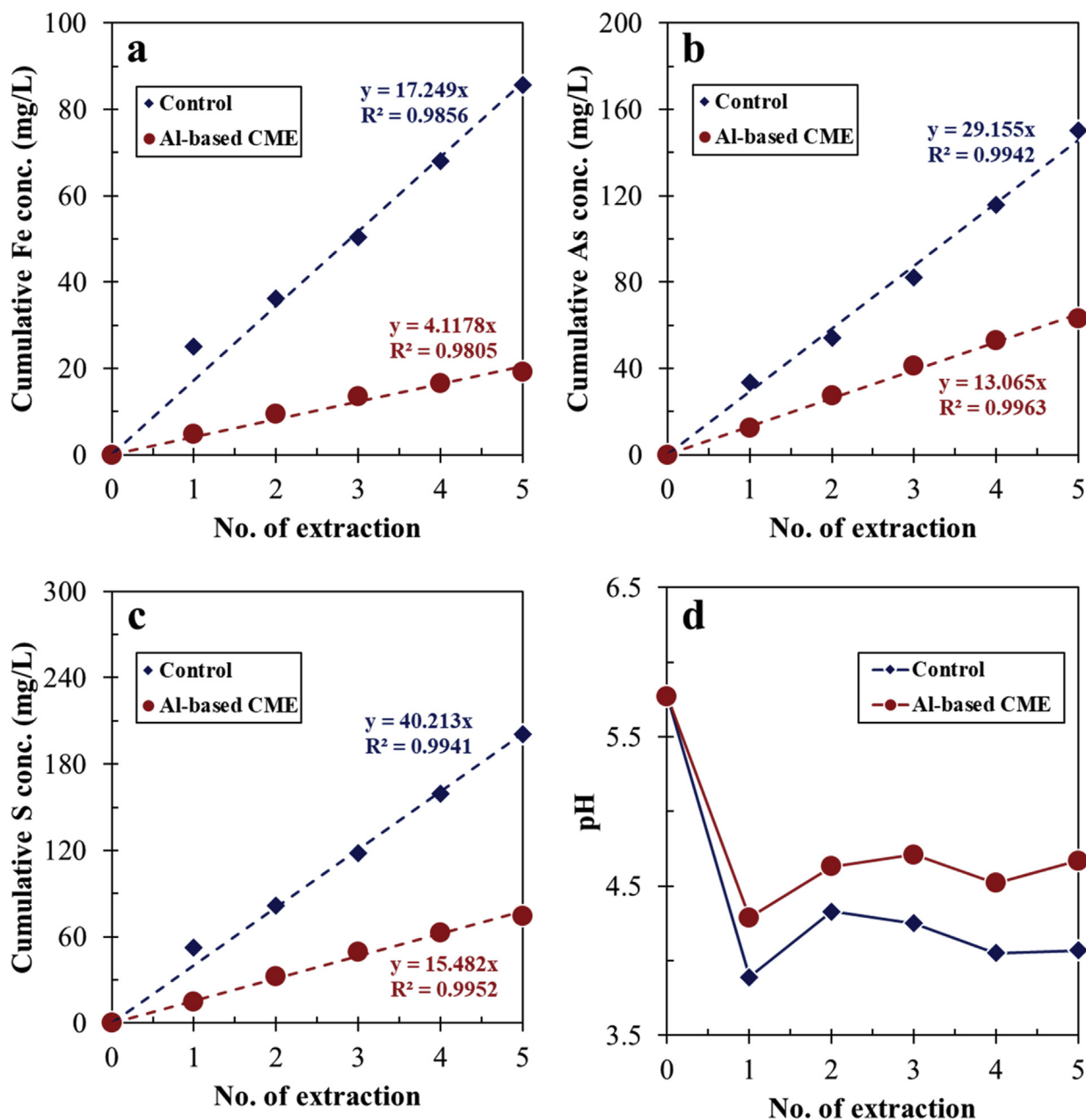


Figure 6. Consecutive batch leaching of arsenopyrite treated in control and by Al-based CME: cumulative concentrations of (a) Fe, (b) As, and (c) S, and (d) evolution of leachate pH vs. the number of extractions.

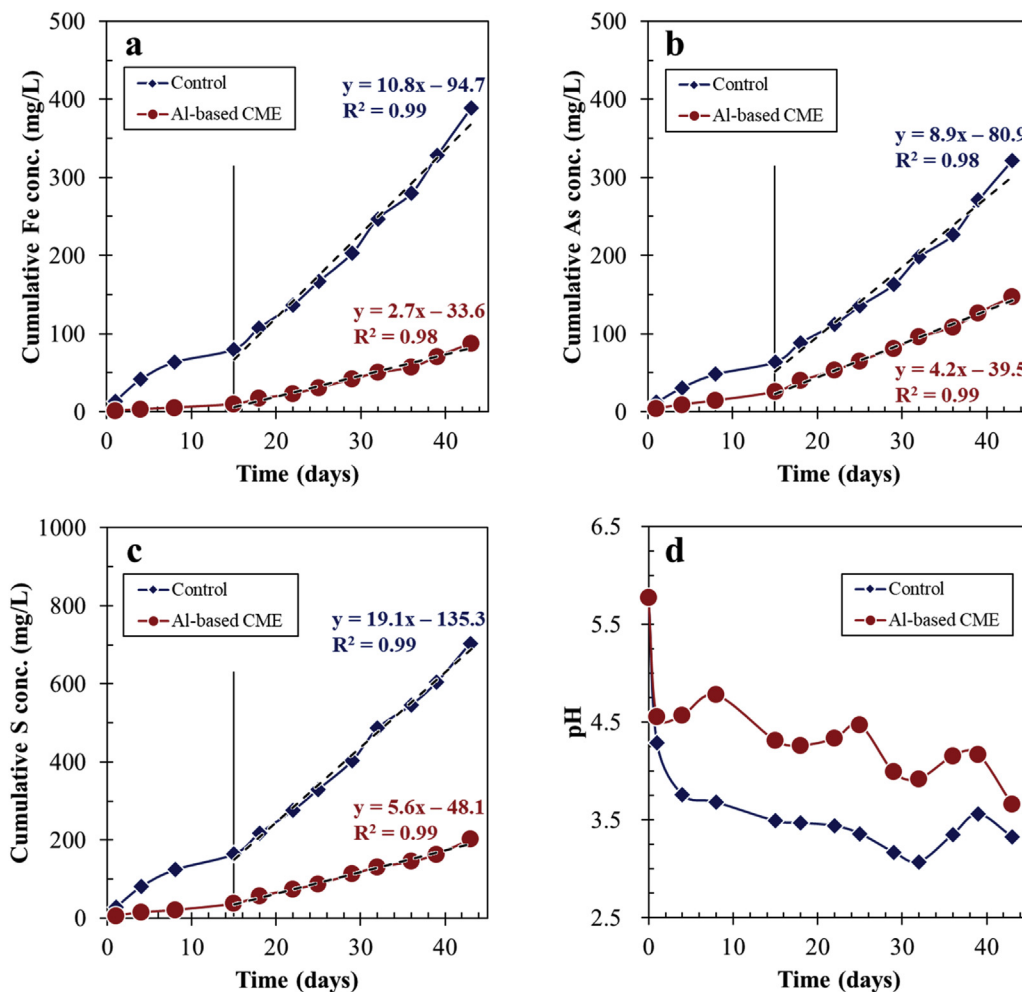


Figure 7. Weathering cell tests of arsenopyrite treated in the control and by Al-based CME: cumulative concentrations of (a) Fe, (b) As, and (c) S, and (d) evolution of leachate pH with time.

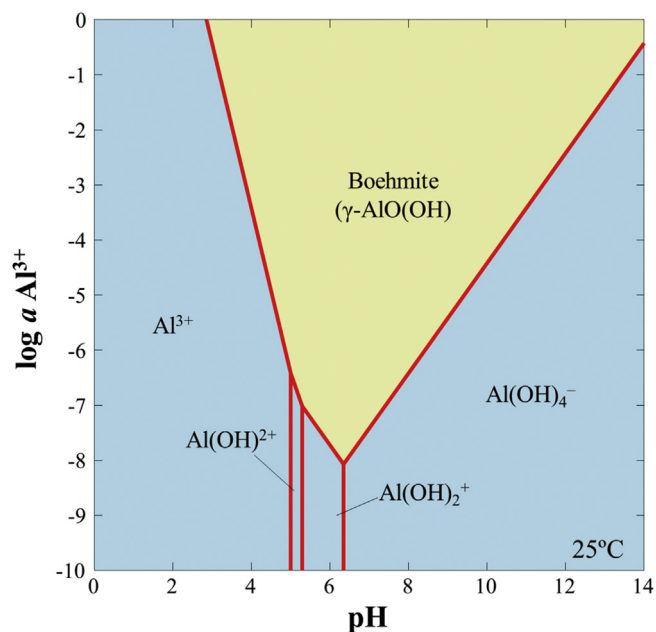


Figure 8. Log activity-pH predominance diagram of Al^{3+} at 25 °C and 1.013 bar created using the Geochemist's Workbench[®] with the MINTEQA2 database (Gustafsson, 2010).

Nonetheless, the extent of arsenopyrite oxidation was significantly lower after Al-based CME than that of the control; that is, the total amounts of Fe, As and S released from arsenopyrite after CME treatment decreased by up to 78, 58 and 63%, respectively. Moreover, Al-based CME lowered the acid generation potential of arsenopyrite as shown in Figure 6d. In the control, pH values of the leachates ranged from 3.9 to 4.3 but those from the Al-based CME-treated arsenopyrite were higher by about 0.5 pH unit.

It is interesting to note that the oxidation of arsenopyrite in the control was more extensive than that treated by Al-based CME even though the mineral in the control was covered with a relatively thicker layer of oxidation products (Figures 2, 3, and 4). As shown in Figure 2, the layer formed on arsenopyrite treated in the control was flaky and had numerous cracks, which allows reactants (e.g., O_2 , Fe^{3+} and H_2O) and products (e.g., $Fe^{2+/3+}$, $As^{3+/5+}$ and SO_4^{2-}) to move freely between the mineral surface and bulk solution. This is most likely the reason why during the consecutive leaching experiments, oxidation of arsenopyrite treated in the control was more substantial than that treated by Al-based CME. Although insightful, consecutive batch leaching tests typically overestimate the release of contaminants from samples because in actual tailings dams and impoundments, agitation or mixing of the mineral-water system is absent (Li et al., 2016; Tabein et al., 2014c). Because of this, weathering cell tests were also conducted to evaluate the stability of Al-based CME-treated arsenopyrite under weathering conditions closer to those encountered in tailings dams and impoundments. As illustrated in Figure 7a–c, the leaching trends of dissolved Fe, As and S in the control increased almost linearly with time during the

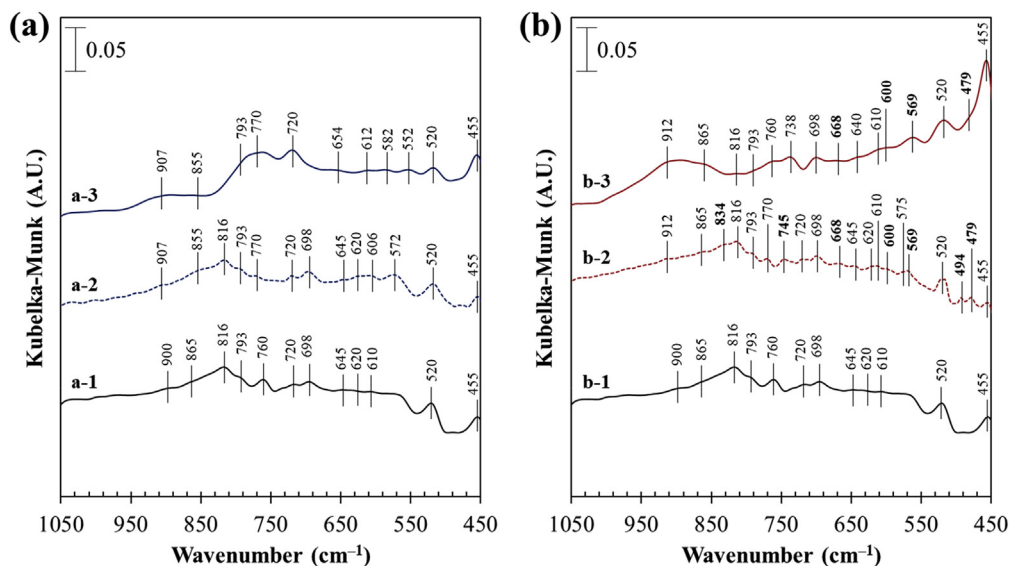


Figure 9. DRIFT spectra of (a-1) fresh arsenopyrite, (a-2) control-treated arsenopyrite before and (a-3) after weathering cell test, (b-1) fresh arsenopyrite, (b-2) Al-based CME-treated arsenopyrite before and (b-3) after weathering cell test. Note that Figure 9a-1, a-2, b-1, and b-2 are adapted from Park et al. (2018d).

weathering cell tests. In comparison, the concentrations of dissolved Fe, As and S in Al-based CME-treated arsenopyrite were relatively low and constant until about 15 days. After this, the leaching concentrations of these three elements started to gradually increase with time but at a relatively slower rate than the control as illustrated by the slopes of the leaching curves (Figure 7a–c). At the end of the weathering tests, cumulative Fe, As and S concentrations leached from arsenopyrite treated in the control were around 390, 320 and 700 mg/L, respectively while those from the Al-based CME-treated arsenopyrite significantly decreased by up to about 80% for Fe, 60% for As, and 70% for S. As noted above, Al-based CME limited the oxidation of arsenopyrite up to about 15 days after which, the suppressive effects of the Al-oxyhydroxide coating gradually declined. The effectiveness of the coating decreased most likely because of the increasing acidity of the system as illustrated in Figure 7d. The leachate pH of Al-based CME-treated arsenopyrite dropped below 4.5 after 15 days that likely enhanced the dissolution of the Al-oxyhydroxide coating as explained by the activity-pH diagram of Al^{3+} illustrated in Figure 8.

Figure 9 shows the DRIFT spectra of arsenopyrite samples treated in control and by Al-based CME before and after the weathering cell tests. The spectra of fresh arsenopyrite (untreated) and that treated in the control (Figure 9a-1 and a-2) showed several IR signatures assigned to arsenopyrite at 455 cm^{-1} (Fe–As vibration) (Achimovičová and Baláz, 2005; Monte et al., 2002) and oxidation products like iron-oxyhydroxides/oxides (900 , 760 , 720 , 698 , 575 and 520 cm^{-1}) (Carlson et al., 2002; Raade et al., 1984; Salama et al., 2015; Tabela et al., 2017c), arsenate adsorbed to iron-oxyhydroxides/oxides (865 , 816 , and 793 cm^{-1}) (Achimovičová and Baláz, 2005; Di Iorio et al., 2018; Gomez et al., 2010; Monte et al., 2002; Voegelin and Hug, 2003) and sulfoxo anions (645 , 620 and 610 cm^{-1}) (Evangelou, 1995; Tabela et al., 2017c). After the weathering cell test, stronger IR signatures of iron-oxyhydroxide/oxide (907 , 760 , and 720 cm^{-1}) as well as adsorbed arsenate (855 and 787 cm^{-1}) were observed (Figure 9a-3), indicating that the arsenopyrite treated in the control was oxidized even further. Meanwhile, the DRIFT spectrum of Al-based CME-treated arsenopyrite before the weathering tests showed IR absorption bands of Al-oxyhydroxide at 834 and 745 cm^{-1} (Al=O bending vibrations), 668 and 600 cm^{-1} (angle bending vibrations of $\text{AlO}(\text{OH})$), and 569 , 494 and 479 cm^{-1} (Angle deformations of $\text{AlO}(\text{OH})$) (Musić et al., 1999; Ram, 2001) (Figure 9b-2), which are consistent with the formation of a bayerite-gibbsite-boehmite coating on arsenopyrite as discussed earlier.

After the weathering cell test, the relative intensities of Al-oxyhydroxide IR signatures either weakened or disappeared (Figure 9b-3), which supports the authors' earlier deduction that the bayerite-gibbsite-boehmite coating formed on arsenopyrite was gradually dissolved due to the increasing acidity of the system (Figure 7d).

To prolong the suppression of Al-based CME-treated arsenopyrite, it is recommended that some pH control mechanism like co-disposal and blending with acid-consuming minerals (e.g., limestone (CaCO_3), dolomite ($\text{CaMg}(\text{CO}_3)_2$), apatite ($\text{Ca}_{10}(\text{PO}_4)_6(\text{OH})_2$) or industrial by-products (e.g., cement kiln dust (CKD) and pulp/paper residue) be incorporated prior to disposal to maintain the pH at around 5–8 where the Al-oxyhydroxide coating is stable. Another option for improving the coating stability could be achieved by increasing its thickness. Assuming that (1) the shape of arsenopyrite is sphere, (2) all the precipitates are present on arsenopyrite, and (3) Al-precipitates are considered as boehmite ($\gamma\text{-AlO}(\text{OH})$), the thickness of coating was theoretically calculated to be around 324 nm . During CME treatment, if the problematic minerals like arsenopyrite and pyrite are covered with thicker coatings, their oxidations in the natural environment would be more effectively curbed.

4. Conclusions

This study investigated in detail the nature of the surface coating formed on arsenopyrite after Al-based CME treatment, including its effects on the electrochemical properties of arsenopyrite and the coating's stability under simulated weathering conditions. The findings of this study are summarized as follows:

- 1) The oxidation of arsenopyrite in the control generated large amounts of secondary products like iron(III)-oxyhydroxide with adsorbed arsenite and arsenate that had “cracky” and flaky surface morphology.
- 2) The surface of CME-treated arsenopyrite was less oxidized because it was covered with an evenly distributed and almost crack-free coating composed of bayerite ($\alpha\text{-Al}(\text{OH})_3$), gibbsite ($\gamma\text{-Al}(\text{OH})_3$), and boehmite ($\gamma\text{-AlO}(\text{OH})$).
- 3) Cyclic voltammetry and chronoamperometry measurements of CME-treated arsenopyrite showed that both the anodic and cathodic half-cell reactions of arsenopyrite oxidation were suppressed due to the insulating Al-based coating.

- 4) CME-treated arsenopyrite suppressed the release of Fe, As and S from arsenopyrite by up to about 80, 60 and 70%, respectively.
- 5) During the weathering cell test, the Al-oxyhydroxide coating on arsenopyrite gradually dissolved with time because of the increasingly acidic conditions of the system.
- 6) Stability of the coatings may be improved by blending CME-treated arsenopyrite with acid-consuming materials to maintain the appropriate pH conditions at around 5 to 8 where Al-oxyhydroxides are stable.

Declarations

Author contribution statement

Ilhwan Park: Conceived and designed the experiments; Performed the experiments; Analyzed and interpreted the data; Contributed reagents, materials, analysis tools or data; Wrote the paper.

Carlito Baltazar Tabelin, Sanghee Jeon, Mayumi Ito, Naoki Hiroyoshi: Conceived and designed the experiments; Analyzed and interpreted the data.

Kensuke Seno: Performed the experiments.

Hiroyuki Inano: Contributed reagents, materials, analysis tools or data.

Funding statement

This work was supported by the Japan Society for the Promotion of Science (JSPS) grant-in-aid for scientific research (Grant numbers: 26820390, JP17H03503 and JP17K12831).

Competing interest statement

The authors declare no conflict of interest.

Additional information

No additional information is available for this paper.

References

Abbassi, R., Khan, F., Hawboldt, K., 2009. Prediction of minerals producing acid mine drainage using a computer-assisted thermodynamic chemical equilibrium model. *Mine Water Environ.* 28 (1), 74–78.

Abdel-Samad, H., Watson, P.R., 1997. An XPS study of the adsorption of chromate on goethite (α -FeOOH). *Appl. Surf. Sci.* 108, 371–377.

Açai, P., Sorrenti, E., Gorner, T., Polaković, M., Kongolo, M., de Donato, P., 2009. Pyrite passivation by humic acid investigated by inverse liquid chromatography. *Colloids Surf., A* 337, 39–46.

Achimovičová, M., Baláz, P., 2005. Influence of mechanical activation on selectivity of acid leaching of arsenopyrite. *Hydrometallurgy* 77 (1–2), 3–7.

Almeida, C.M.V.B., Giannetti, B.F., 2003. Electrochemical study of arsenopyrite weathering. *Phys. Chem. Chem. Phys.* 5 (3), 604–610.

Bouzahzah, H., Benzaazoua, M., Bussiere, B., Plante, B., 2014. Prediction of acid mine drainage: importance of mineralogy and the test protocols for static and kinetic tests. *Mine Water Environ.* 33, 54–65.

Buckley, A.N., Walker, G.W., 1988. The surface composition of arsenopyrite exposed to oxidizing environments. *Appl. Surf. Sci.* 35, 227–240.

Cai, M.-F., Dang, Z., Chen, Y.-W., Belzile, N., 2005. The passivation of pyrrhotite by surface coating. *Chemosphere* 61 (5), 659–667.

Carlson, L., Bigham, J.M., Schwertmann, U., Kyeck, A., Wagner, F., 2002. Scavenging of as from acid mine drainage by schwertmannite and ferrihydrite: a comparison with synthetic analogues. *Environ. Sci. Technol.* 36 (8), 1712–1719.

Chopard, A., Benzaazoua, M., Bouzahzah, H., Plante, B., Marion, P., 2017. A contribution to improve the calculation of the acid generating potential of mining wastes. *Chemosphere* 175, 97–107.

Corkhill, C.L., Vaughan, D.J., 2009. Arsenopyrite oxidation – a review. *Appl. Geochem.* 24 (12), 2342–2361.

Crundwell, F.K., 1988. The influence of the electronic structure of solids on the anodic dissolution and leaching of semiconducting sulphide minerals. *Hydrometallurgy* 21 (2), 155–190.

Di Iorio, E., Cho, H.G., Liu, Y., Cheng, Z., Angelico, R., Colombo, C., 2018. Arsenate retention mechanisms on hematite with different morphologies evaluated using AFM, TEM measurements and vibrational spectroscopy. *Geochem. Cosmochim. Acta* 237, 155–170.

Ding, M., De Jong, B.H.W.S., Roosendaal, S.J., Vredenberg, A., 2000. XPS studies on the electronic structure of bonding between solid and solutes: adsorption of arsenate, chromate, phosphate, Pb^{2+} , and Zn^{2+} ions on amorphous black ferric oxyhydroxide. *Geochem. Cosmochim. Acta* 64 (7), 1209–1219.

Dos Santos, E.C., de Mendonça Silva, J.C., Duarte, H.A., 2016. Pyrite oxidation mechanism by oxygen in aqueous medium. *J. Phys. Chem. C* 120, 2760–2768.

Duker, A.A., Carranza, E.J.M., Hale, M., 2005. Arsenic geochemistry and health. *Environ. Int.* 31 (5), 631–641.

Elderfield, H., Hem, J.D., 1973. The development of crystalline structure in aluminum hydroxide polymorphs on ageing. *Miner. Mag.* 89–96.

Elsetinow, A.R., Borda, M.J., Schoonen, M.A.A., Strongin, D.R., 2003. Suppression of pyrite oxidation in acidic aqueous environments using lipids having two hydrophobic tails. *Adv. Environ. Res.* 7, 969–974.

Evangelou, V.P., 1995. Pyrite Oxidation and its Control. CRC press, Boca Raton, FL.

Evangelou, V.P., 1996. Oxidation Proof Silicate Surface Coating on Iron Sulfides. U.S. Patent No. 5,494,703.

Frau, F., Rossi, A., Ardaù, C., Biddau, R., Pelo, S.D., Atzei, D., Licheri, C., Cannas, C., Capitani, G.C., 2005. Determination of arsenic speciation in complex environmental samples by the combined use of TEM and XPS. *Microchim. Acta* 151, 189–201.

Gazea, B., Adam, K., Kontopoulos, A., 1996. A review of passive systems for the treatment of acid mine drainage. *Miner. Eng.* 9 (1), 23–42.

Gomez, M.A., Assaoudi, H., Becze, L., Cutler, J.N., Demopoulos, G.P., 2010. Vibrational spectroscopy study of hydrothermally produced scorodite ($FeAsO_4 \cdot 2H_2O$), ferric arsenate sub-hydrate (FASh; $FeAsO_4 \cdot 0.75H_2O$) and basic ferric arsenate sulfate (BFAS; $Fe[(AsO_4)_{1-x}(SO_4)_x(OH)_x] \cdot nH_2O$). *J. Raman Spectrosc.* 41, 212–221.

Gustafsson, J.P., 2010. Visual MINTEQ Thermodynamic Database in GWB Format. <http://vminetq.lwr.kth.se>. (Accessed 9 December 2018).

Habib, K., 2016. Surface resistivity/conductivity of oxide-hydroxide compounds in inhibited seawater by optical interferometry. *J. Saudi Chem. Soc.* 20, S541–S546.

Heo, Y., Im, H., Kim, J., Kim, J., 2012. The influence of Al(OH)₃-coated graphene oxide on improved thermal conductivity and maintained electrical resistivity of Al₂O₃/epoxy composites. *J. Nanoparticle Res.* 14, 1196, 1–10.

Herrera, P., Uchiyama, H., Igarashi, T., Asakura, K., Ochi, Y., Iyatomi, N., Nagae, S., 2007. Treatment of acid mine drainage through a ferrite formation process in central Hokkaido, Japan: evaluation of dissolved silica and aluminum in ferrite formation. *Miner. Eng.* 20, 1255–1260.

Hsu, P.H., 1966. Formation of gibbsite from aging hydroxy-aluminum solutions. *Soil Sci. Soc. Am. J.* 30, 173–176.

Huang, X., Evangelou, V.P., 1992. Abatement of Acid Mine Drainage by Encapsulation of Acid Producing Geologic Materials. U.S. Department of the Interior, Bureau of Mines. Contact No. J0309013.

Huo, L., Zeng, X., Su, S., Bai, L., Wang, Y., 2017. Enhanced removal of as (V) from aqueous solution using modified hydrous ferric oxide nanoparticles. *Sci. Rep.* 7, 40765.

Igarashi, T., Imagawa, H., Uchiyama, H., Asakura, K., 2008. Leaching behavior of arsenic from various rocks by controlling geochemical conditions. *Miner. Eng.* 21, 191–199.

Jha, R.K.T., Satur, J., Hiroyoshi, N., Ito, M., Tsunekawa, M., 2008. Carrier-microencapsulation using Si-catechol complex for suppressing pyrite floatability. *Miner. Eng.* 21, 889–893.

Johnson, D.B., Hallberg, K.B., 2005. Acid mine drainage remediation options: a review. *Sci. Total Environ.* 338 (1–2), 3–14.

Kefeni, K.K., Msagati, T.M., Mamba, B.B., 2015. Synthesis and characterization of magnetic nanoparticles and study their removal capacity of metals from acid mine drainage. *Chem. Eng. J.* 276, 222–231.

Khummalai, N., Boonamnuayvitaya, V., 2005. Suppression of arsenopyrite surface oxidation by sol-gel coatings. *J. Biosci. Bioeng.* 99 (3), 277–284.

Kloprogge, J.T., Duong, L.V., Wood, B.J., Frost, R.L., 2006. XPS study of the major minerals in bauxite: gibbsite, bayerite and (pseudo-)boehmite. *J. Colloid Interface Sci.* 296, 572–576.

Kloprogge, J.T., Wood, B.J., 2016. Systematic XPS study of gallium-substituted boehmite. *J. Mater. Sci.* 51 (11), 5436–5444.

Lara, R.H., Velázquez, L.J., Vázquez-Arenas, J., Mallet, M., Dossot, M., Labastida, I., Sosa-Rodríguez, F.S., Espinosa-Cristóbal, L.F., Escobedo-Bretado, M.A., Cruz, R., 2016. Arsenopyrite weathering under conditions of simulated calcareous soil. *Environ. Sci. Pollut. Res.* 23, 3681–3706.

Lee, Y.-P., Liu, Y.-H., Yeh, C.-S., 1999. Formation of bayerite, gibbsite and boehmite particles by laser ablation. *Phys. Chem. Chem. Phys.* 1, 4681–4686.

Li, J., Kosugi, T., Riya, S., Hashimoto, Y., Hou, H., Terada, A., Hosomi, M., 2016. Potential for leaching of arsenic from excavated rock after different drying treatments. *Chemosphere* 154, 276–282.

Li, X., Hiroyoshi, N., Tabelin, C.B., Naruwa, K., Harada, C., Ito, M., 2019. Suppressive effects of ferric-catecholate complexes on pyrite oxidation. *Chemosphere* 214, 70–78.

Liu, Y., Hu, X., Xu, Y., 2017. PropS-SH/SiO₂ nanocomposite coatings for pyrite oxidation inhibition to control acid mine drainage at the source. *J. Hazard Mater.* 338, 313–322.

Mohan, D., Pittman, C.U., 2007. Arsenic removal from water/wastewater using adsorbents – a critical review. *J. Hazard Mater.* 142 (1–2), 1–53.

Monte, M.B.M., Butra, A.J.B., Albuquerque, C.R.F., Tondo, L.A., Lins, F.F., 2002. The influence of the oxidation state of pyrite and arsenopyrite on the flotation of an auriferous sulphide ore. *Miner. Eng.* 15 (12), 1113–1120.

Murciego, A., Álvarez-Ayuso, E., Pellitero, E., Rodríguez, M.A., García-Sánchez, A., Tamayo, J., Rubio, J., Rubio, F., Rubin, J., 2011. Study of arsenopyrite weathering products in mine wastes from abandoned tungsten and tin exploitations. *J. Hazard Mater.* 186, 590–601.

Musić, S., Dragčević, D., Popović, S., 1999. Hydrothermal crystallization of boehmite from freshly pre-cipitated aluminium hydroxide. *Mater. Lett.* 40 (6), 269–274.

- Nesbitt, H.W., Muir, I.J., 1994. X-ray photoelectron spectroscopic study of a pristine pyrite surface reacted with water vapour and air. *Geochem. Cosmochim. Acta* 58, 4667–4679.
- Nesbitt, H.W., Muir, I.J., Pratt, A.R., 1995. Oxidation of arsenopyrite by air and air-saturated, distilled water, and implications for mechanism of oxidation. *Geochem. Cosmochim. Acta* 59 (9), 1773–1786.
- Ouyang, Y., Liu, Y., Zhu, R., Ge, F., Xu, T., Luo, Z., Liang, L., 2015. Pyrite oxidation inhibition by organosilane coatings for acid mine drainage control. *Miner. Eng.* 72, 57–64.
- Park, C.K., Kim, J.W., Jung, M.C., Park, H.S., Kim, D.K., Oh, Y.S., 2018a. Current occurrence and heavy metal contamination assessment of seepage from mine waste dumping sites in Korea. *J. Korean Soc. Miner. Energy Resour. Eng.* 55 (6), 588–595.
- Park, J., Park, I., Oh, J., Yoo, K., 2018b. Behaviors of cyanide leaching of gold in tailings and adsorption of gold ions on activated carbon. *J. Korean Soc. Miner. Energy Resour. Eng.* 55 (5), 414–420.
- Park, I., Tabelin, C.B., Magaribuchi, K., Seno, K., Ito, M., Hiroyoshi, N., 2018c. Suppression of the release of arsenic from arsenopyrite by carrier-microencapsulation using Ti-catechol complex. *J. Hazard Mater.* 344, 322–332.
- Park, I., Tabelin, C.B., Seno, K., Jeon, S., Ito, M., Hiroyoshi, N., 2018d. Simultaneous suppression of acid mine drainage formation and arsenic release by Carrier-microencapsulation using aluminum-catecholate complexes. *Chemosphere* 205, 414–425.
- Park, I., Tabelin, C.B., Jeon, S., Li, X., Seno, K., Ito, M., Hiroyoshi, N., 2019a. A review of recent strategies for acid mine drainage prevention and mine tailings recycling. *Chemosphere* 219, 588–606.
- Park, I., Tabelin, C., Inano, H., Seno, K., Higuchi, K., Ito, M., Hiroyoshi, N., 2019b. Formation of surface protective coatings on arsenopyrite using Al-catecholate complex and its mode of inhibition of arsenopyrite oxidation. *MATEC Web Conf.* 268, 06015.
- Raade, G., Mladek, M.H., Kristiansen, R., Din, V.K., 1984. Kaatialaite, a new ferric arsenate mineral from Finland. *Am. Mineral.* 69, 383–387.
- Ram, S., 2001. Infrared spectral study of molecular vibrations in amorphous, nanocrystalline and $\text{AlO}(\text{OH})\cdot\alpha\text{-H}_2\text{O}$ bulk crystals. *Infrared Phys. Technol.* 42 (6), 547–560.
- Rimstidt, J.D., Vaughan, D.J., 2003. Pyrite oxidation: a state-of-the-art assessment of the reaction mechanism. *Geochem. Cosmochim. Acta* 67 (5), 873–880.
- Ruan, H.D., Frost, R.L., Klopogge, J.T., 2001. Comparison of Raman spectra in characterizing gibbsite, bayerite, diasporite and boehmite. *J. Raman Spectrosc.* 32, 745–750.
- Salama, W., Aref, M.E., Gaupp, R., 2015. Spectroscopic characterization of iron ores formed in different geological environments using FTIR, XPS, Mössbauer spectroscopy and thermoanalyses. *Spectrochim. Acta A Mol. Biomol. Spectrosc.* 136, 1816–1826.
- Satur, J., Hiroyoshi, N., Tsunekawa, M., Ito, M., Okamoto, H., 2007. Carrier-microencapsulation for preventing pyrite oxidation. *Int. J. Miner. Process.* 83, 116–124.
- Seno, K., Park, I., Tabelin, C., Magaribuchi, K., Ito, M., Hiroyoshi, N., 2019. Carrier-microencapsulation using Al-catecholate complex to suppress arsenopyrite oxidation: evaluation of the coating stability under simulated weathering conditions. *MATEC Web Conf.* 268, 06002.
- Shirley, D.A., 1972. High-resolution X-ray photoemission spectrum of the valence bands of gold. *Phys. Rev. B* 5, 4709–4714.
- Tabelin, C.B., Igarashi, T., 2009. Mechanisms of arsenic and lead release from hydrothermally altered rock. *J. Hazard Mater.* 169, 980–990.
- Tabelin, C.B., Igarashi, T., Tamoto, S., 2010. Factors affecting arsenic mobility from hydrothermally altered rock in impoundment-type in situ experiments. *Miner. Eng.* 23, 238–248.
- Tabelin, C.B., Igarashi, T., Takahashi, R., 2012a. Mobilization and speciation of arsenic from hydrothermally altered rock in laboratory column experiments under ambient conditions. *Appl. Geochem.* 27, 326–342.
- Tabelin, C.B., Igarashi, T., Yoneda, T., 2012b. Mobilization and speciation of arsenic from hydrothermally altered rock containing calcite and pyrite under anoxic conditions. *Appl. Geochem.* 27, 2300–2314.
- Tabelin, C.B., Igarashi, T., Tamoto, S., Takahashi, R., 2012c. The roles of pyrite and calcite in the mobilization of arsenic and lead from hydrothermally altered rocks excavated in Hokkaido, Japan. *J. Geochem. Explor.* 119–120, 17–31.
- Tabelin, C.B., Basri, A.H.M., Igarashi, T., Yoneda, T., 2012d. Removal of arsenic, boron, and selenium from excavated rocks by consecutive washing. *Water Air Soil Pollut.* 223, 4153–4167.
- Tabelin, C.B., Igarashi, T., Yoneda, T., Tamamura, S., 2013. Utilization of natural and artificial adsorbents in the mitigation of arsenic leached from hydrothermally altered rock. *Eng. Geol.* 156, 58–67.
- Tabelin, C.B., Igarashi, T., Arima, T., Sato, D., Tatsuahara, T., Tamoto, S., 2014a. Characterization and evaluation of arsenic and boron adsorption onto natural geogenic materials, and their application in the disposal of excavated altered rock. *Geoderma* 213, 163–172.
- Tabelin, C.B., Hashimoto, A., Igarashi, T., Yoneda, T., 2014b. Leaching of boron, arsenic and selenium from sedimentary rocks: I. Effects of contact time, mixing speed and liquid-to-solid ratio. *Sci. Total Environ.* 472, 620–629.
- Tabelin, C.B., Hashimoto, A., Igarashi, T., Yoneda, T., 2014c. Leaching of boron, arsenic, and selenium from sedimentary rocks: II. pH dependence, speciation, and mechanisms of release. *Sci. Total Environ.* 473–474, 244–253.
- Tabelin, C.B., Sasaki, R., Igarashi, T., Park, I., Tamoto, S., Arima, T., Ito, M., Hiroyoshi, N., 2017a. Simultaneous leaching of arsenite, arsenate, selenite, and selenate, and their migration in tunnel-excavated sedimentary rocks: I. Column experiments under intermittent and unsaturated flow. *Chemosphere* 186, 558–569.
- Tabelin, C.B., Sasaki, R., Igarashi, T., Park, I., Tamoto, S., Arima, T., Ito, M., Hiroyoshi, N., 2017b. Simultaneous leaching of arsenite, arsenate, selenite, and selenate, and their migration in tunnel-excavated sedimentary rocks: II. Kinetic and reactive transport modeling. *Chemosphere* 188, 444–454.
- Tabelin, C.B., Veerawattanun, S., Ito, M., Hiroyoshi, N., Igarashi, T., 2017c. Pyrite oxidation in the presence of hematite and alumina: I. Batch leaching experiments and kinetic modeling calculations. *Sci. Total Environ.* 580, 687–698.
- Tabelin, C.B., Veerawattanun, S., Ito, M., Hiroyoshi, N., Igarashi, T., 2017d. Pyrite oxidation in the presence of hematite and alumina: II. Effects on the cathodic and anodic half-cell reactions. *Sci. Total Environ.* 581–582, 126–135.
- Tabelin, C.B., Igarashi, T., Villacorte-Tabelin, M., Park, I., Opiso, E.M., Ito, M., Hiroyoshi, N., 2018. Arsenic, selenium, boron, lead, cadmium, copper, and zinc in naturally contaminated rocks: a review of their sources, modes of enrichment, mechanisms of release, and mitigation strategies. *Sci. Total Environ.* 645, 1522–1553.
- Tamoto, S., Tabelin, C.B., Igarashi, T., Ito, M., Hiroyoshi, N., 2015. Short and long term release mechanisms of arsenic, selenium and boron from tunnel-excavated sedimentary rock under in situ conditions. *J. Contam. Hydrol.* 175–176, 60–71.
- Tatsuahara, T., Arima, T., Igarashi, T., Tabelin, C.B., 2012. Combined neutralization-adsorption system for the disposal of hydrothermally altered excavated rock producing acidic leachate with hazardous elements. *Eng. Geol.* 139–140, 76–84.
- Urbano, G., Reyes, V.E., Veloz, M.A., González, I., Cruz, J., 2008. Pyrite-arsenopyrite galvanic interaction and electrochemical reactivity. *J. Phys. Chem. C* 112 (28), 10453–10461.
- Violante, A., Huang, P.M., 1993. Formation mechanism of aluminum hydroxide polymorphs. *Clay Clay Miner.* 41 (5), 590–597.
- Voegelin, A., Hug, S.J., 2003. Catalyzed oxidation of arsenic(III) by hydrogen peroxide on the surface of ferrihydrite: an in situ ATR-FTIR study. *Environ. Sci. Technol.* 37, 972–978.
- Walker, F.P., Schreiber, M.E., Rimstidt, J.D., 2006. Kinetics of arsenopyrite oxidative dissolution by oxygen. *Geochem. Cosmochim. Acta* 70 (7), 1668–1676.
- Yuniati, M.D., Kitagawa, K., Hirajima, T., Miki, H., Okibe, N., Sasaki, K., 2015. Suppression of pyrite oxidation in acid mine drainage by carrier microencapsulation using liquid product of hydrothermal treatment of low-rank coal, and electrochemical behavior of resultant encapsulating coatings. *Hydrometallurgy* 158, 83–93.
- Zhang, Y.L., Evangelou, V.P., 1998. Formation of ferric hydroxide-silica coatings on pyrite and its oxidation behavior. *Soil Sci.* 163 (1), 53–62.
- Zhu, T., Lu, X., Liu, H., Li, J., Zhu, X., Lu, J., Wang, R., 2014. Quantitative X-ray photoelectron spectroscopy-based depth profiling of bioleached arsenopyrite surface by *Acidithiobacillus ferrooxidans*. *Geochem. Cosmochim. Acta* 127, 120–139.